Electronic Supplementary Material (ESI) for Chemical Science.

Supporting Information

Tandem rigidification and π-extension as a key tool for the development of a narrow linewidth yellow hyperfluorescent OLED system.

by Krzysztof Bartkowski, Paola Zimmermann Crocomo, Michał A. Kochman, Dharmandra Kumar, Adam Kubas, Przemysław Data, Marcin Lindner

General Remarks.

All reagents and solvents were purchased from commercial sources and were used as received unless otherwise noted. Reagent grade solvents (CH_2Cl_2, hexane) were distilled prior to use. For water-sensitive reactions solvents were dried using Solvent Purification System from MBraun. Transformations with moisture and oxygen sensitive compounds were performed under a stream of argon. The reaction progress was monitored by means of thin layer chromatography (TLC), which was performed on aluminum foil plates, covered with Silica gel 60 F254 (Merck). Products purification was done by means of column chromatography with Kieselgel 60 (Merck). The identity and purity of prepared compounds were proved by ^1H NMR and ^{13}C NMR spectrometry as well as by MS spectrometry (via EI-MS) and IR spectroscopy. NMR spectra were measured on Bruker AM 500 MHz, Bruker AM 600 MHz or Varian 600 MHz instruments with TMS as internal standard. Chemical shifts for ^1H NMR are expressed in parts per million (ppm) relative to tetramethylsilane (δ 0.00 ppm), $CDCl_3$ (δ 7.26 ppm) or CD_2Cl_2 (δ 5.32 ppm). Chemical shifts for ^{13}C NMR are expressed in ppm relative to $CDCl_3$ (δ 77.16 ppm) or CD_2Cl_2 (δ 54.00 ppm). Data are reported as follows: chemical shift, multiplicity (s = singlet, d = doublet, dd = doublet of doublets, t = triplet, m = multiplet), coupling constant (Hz), and integration. EI mass spectra were obtained on AutoSpec Premier spectrometer. IR spectra were recorded on JASCO FT/IR-6200 spectrometer.

Synthetic procedures

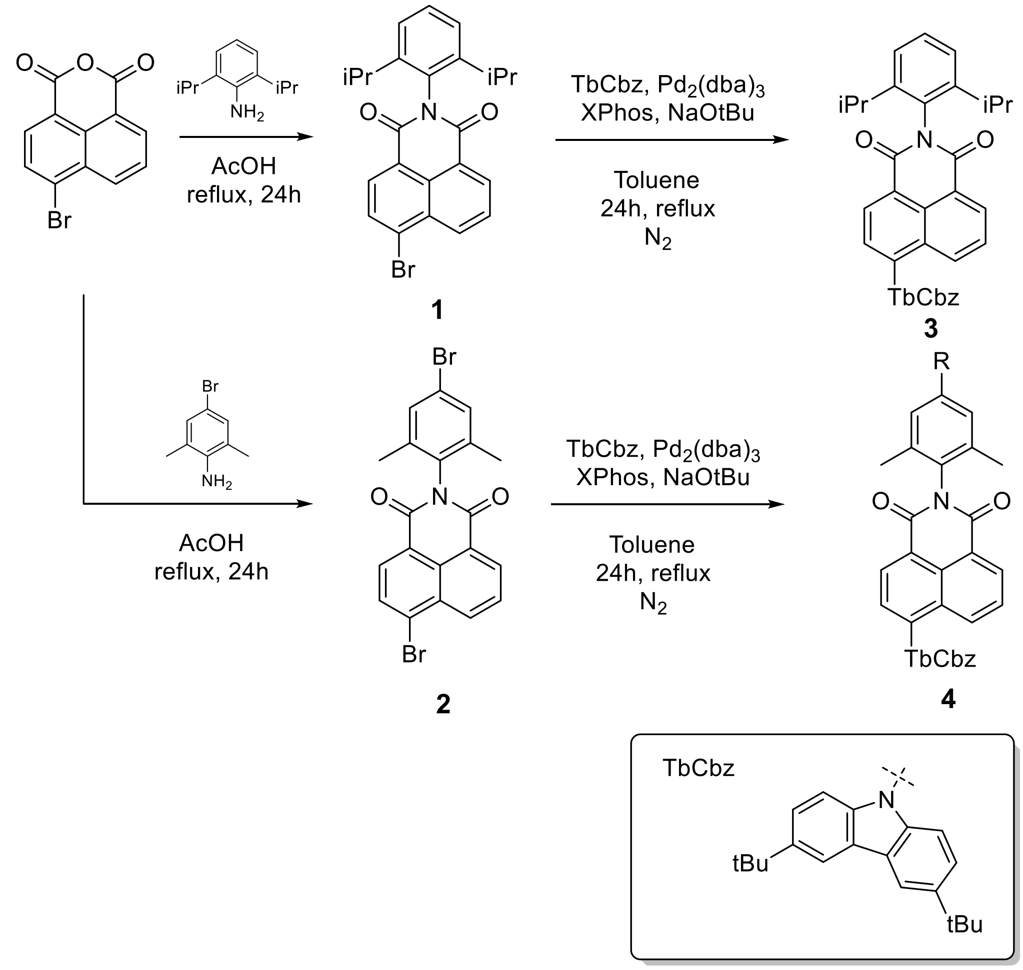
1 2 3 4

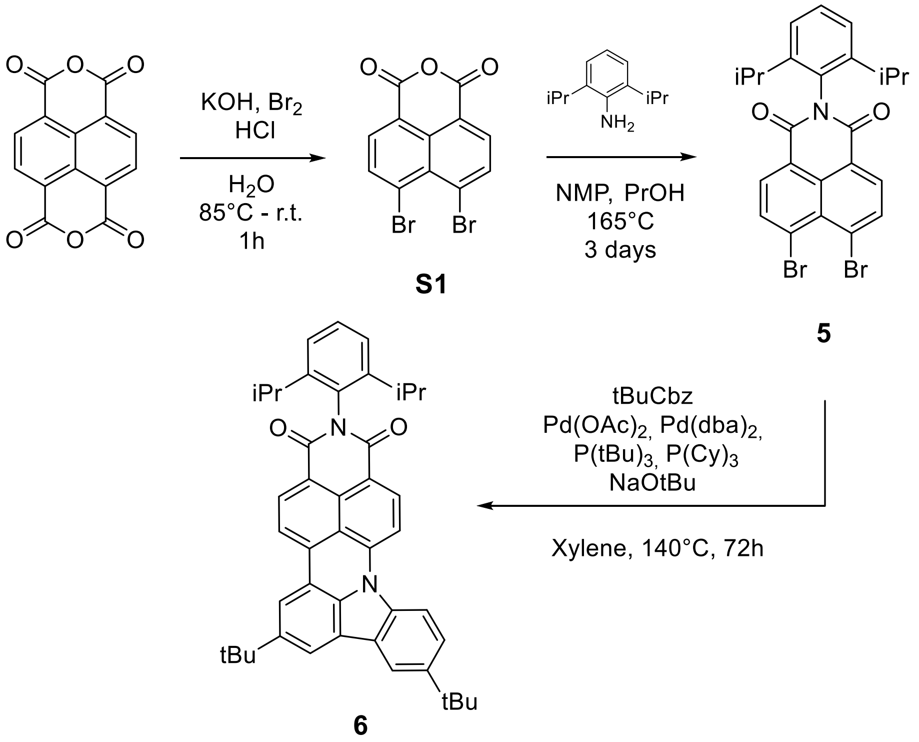
S1 5 6

Compounds **1, 3, S1** and **5** were synthesized according to the known procedures. Spectral data were consistent with previously reported. [1,2]

General procedure of Buchwald-Hartwig coupling: In heat-gun heated, argon flushed pressure tube 150 mg (1 eq) of **1/2** was dissolved in 20mL of anhydrous toluene. To this solution 1.05 or 2.1 eq of 3,6-di*tert*butylcarbazole was added, followed by 1.05/2.1 eq of NaOtBu, 0.2/0.4 eq of XPhos and 0.1/0.2 eq of Pd$_2$(dba)$_3$. Mixture was vigorously purged by Ar and closed. After overnight heating in 115°C solution was cooled to room temperature and solvent was evaporated. The residue was dissolved in DCM and suspended on Celite. The purification by column chromatography (silica gel, hexane/DCM 1/1, with 1% of Et$_3$N) followed by recrystallization from DCM/methanol system led to obtain expected products with various yields.

6-(3,6-di-*tert*-butyl-9H-carbazol-9-yl)-2-(2,6-diisopropylphenyl)-1H-benzo[de]isoquinoline-1,3(2H)-dione (**2**). Yellow solid, 156 mg, 71%. **^{1}H NMR (500 MHz, 300K, CDCl$_3$)** δ (ppm) 8.82 (d, J=7.7Hz, 1H), 8.73 (dd, ^{3}J=7.2Hz,^{4}J= 1.2Hz, 1H), 8.23 (d, J=1.9Hz, 2H), 8.00 (dd, ^{3}J=8.5Hz, ^{4}J=1.2Hz, 1H), 7.92 (d, J=7.8Hz, 1H), 7.68 (dd, ^{3}J=8.5Hz, ^{4}J=7.2Hz, 1H), 7.53 –7.46 (m, 1H), 7.43 (dd, ^{3}J=8.7Hz, ^{4}J=2.0Hz, 2H), 7.36 (d, J=7.8Hz, 2H), 7.04 (d, J=8.6Hz, 2H), 2.89 – 2.77 (m, 2H), 1.49 (s, 18H), 1.22 (dd, ^{3}J=6.9Hz, ^{4}J=4.3Hz, 12H). **^{13}C NMR (126 MHz,300K, CDCl$_3$)** δ (ppm) 164.0, 163.6, 145.7, 143.9, 141.4, 140.2, 132.4, 132.1, 130.8, 130.7, 130.3, 129.6, 129.2, 127.5, 127.0, 124.1, 124.0, 124.0, 123.4, 122.2, 116.6, .109.6, 77.3, 77.0, 76.8, 34.8, 32.0, 29.2, 24.1, 24.1. **HRMS (ESI, m/z)** 657.3458 [M+Na]$^+$ (calc. for $C_{44}H_{46}N_2O_2Na$ 657.3457). **IR (KBr)** ν (cm^{-1}) 3065, 2960, 2868, 1712, 1672, 1588, 1476, 1363,1236, 807, 785.

6-(3,6-di-*tert*-butyl-9*H*-carbazol-9-yl)-2-(4-(3,6-di-*tert*-butyl-9*H*-carbazol-9-yl)-2,6-dimethylphenyl)-1*H*-benzo[*de*]isoquinoline-1,3(2*H*)-dione (**4**). Yellow solid. 161mg, 59%. **^{1}H NMR (600MHz, 300K, CD$_2$Cl$_2$)** δ (ppm) 8.87 (d, J=7.6Hz, 1H), 8.76 (dd, ^{3}J=7.1Hz, ^{4}J=1.1Hz, 1H), 8.27 (d, J=1.7Hz, 2H), 8.20 (d, J=1.7Hz, 2H), 7.99 (dd, ^{3}J=8.6Hz, ^{4}J=1.0Hz, 1H), 7.98 (d, J=7.7Hz, 1H), 7.73 (dd, ^{3}J=8.3Hz, ^{4}J=7.3Hz, 1H), 7.55-7.46 (m, 8H), 7.05 (dd, J=8.7Hz, 2H), 2.31 (s, 6H), 1.495 (s, 18H), 1.490 (s, 18H). **^{13}C NMR (150MHz, 300K, CD$_2$Cl$_2$)** δ (ppm) 163.4, 162.9, 143.8, 141.4, 140.2, 138.9, 139.2, 137.7, 132.7, 132.4, 132.0, 130.9, 130.4, 129.2, 127.5, 127.1, 125.9, 124.0, 123.8, 123.6, 123.4, 123.37, 122.2, 116.6, 116.2, 109.5, 109.4, 34.7, 34.6, 31.7, 31.68, 17.9. **HRMS (EI)** 855.4759 (calc. for $C_{60}H_{61}N_3O_2$ 855.4764) **IR (KBr)** ν (cm^{-1}) 3424 (br), 2959, 2903, 2866, 1716, 1678, 1589, 1489, 1477, 1362, 1295, 1235, 1192, 1034, 810.

Buchwald-Hartwig – direct arylation coupling of 6: In heat-gun heated, argon flushed pressure tube 250 mg (1 eq) of **S4** was dissolved in 7 mL of anhydrous toluene. To this solution 2.2 eq of 3,6-di*tert*butylcarbazole was added, followed by 2.4 eq of NaOtBu, 0.1 eq of P(Cy)$_3$, 0.1 eq of P(tBu)$_3$HBF$_4$, 0.05 eq of Pd$_2$(dba)$_3$ and 0.05 eq of Pd(OAc)$_2$. Mixture was virgously purged by Ar, closed and heated at 115°C for 16 h. After cooling down to the room temperature solvent was evaporated and the crude mixture was separated by column chromatography (hexane/DCM 1/2). Desired fraction was evaporated and the solid was washed with pentane. Red solid, 123 mg, 40%. **^{1}H NMR (CD_2Cl_2, 300K, 500MHz)** δ (ppm) 8.72 (d, *J*=3.4Hz, 1H), 8.70 (d, *J*=3.1Hz, 1H), 8.29 (bs, 1H), 8.27-8.24 (m, 4H), 8.13 (d, *J*=8.6Hz, 1H), 7.74 (dd, ^3J=8.8Hz, ^4J=2.0Hz, 1H), 7.49 (t, *J*=7.8Hz, 1H), 7.34 (d, *J*=7.8Hz, 2H), 2.75 (m, 2H), 1.58 (s, 9H), 1.52 (s, 9H), 1.14 (d, *J*=6.8Hz, 12H). **^{13}C NMR (125 MHz, 300K, CD_2Cl_2)** δ 164.2, 163.7, 148.4, 147.4, 146.1, 141.5, 137.0, 136.1, 134.4, 134.0, 132.6, 132.3, 132.1, 129.0, 127.0, 125.5, 124.6, 123.9, 123.4, 119.9, 119.2, 118.1, 115.9, 114.2, 114.0, 107.5, 53.8, 53.6, 53.4, 53.2, 53.0, 35.4, 34.8, 31.6, 31.4, 29.0, 23.7. **HRMS (EI)** 632.3426 (calc. for $C_{44}H_{44}N_2O_2$ 632.3408). **IR (KBr)** ν (cm^{-1}) 2957, 2925, 2866, 1692, 1652, 1585, 1485, 1447, 1347, 1257, 804.

NMR spectra of 2, 4, and 6.

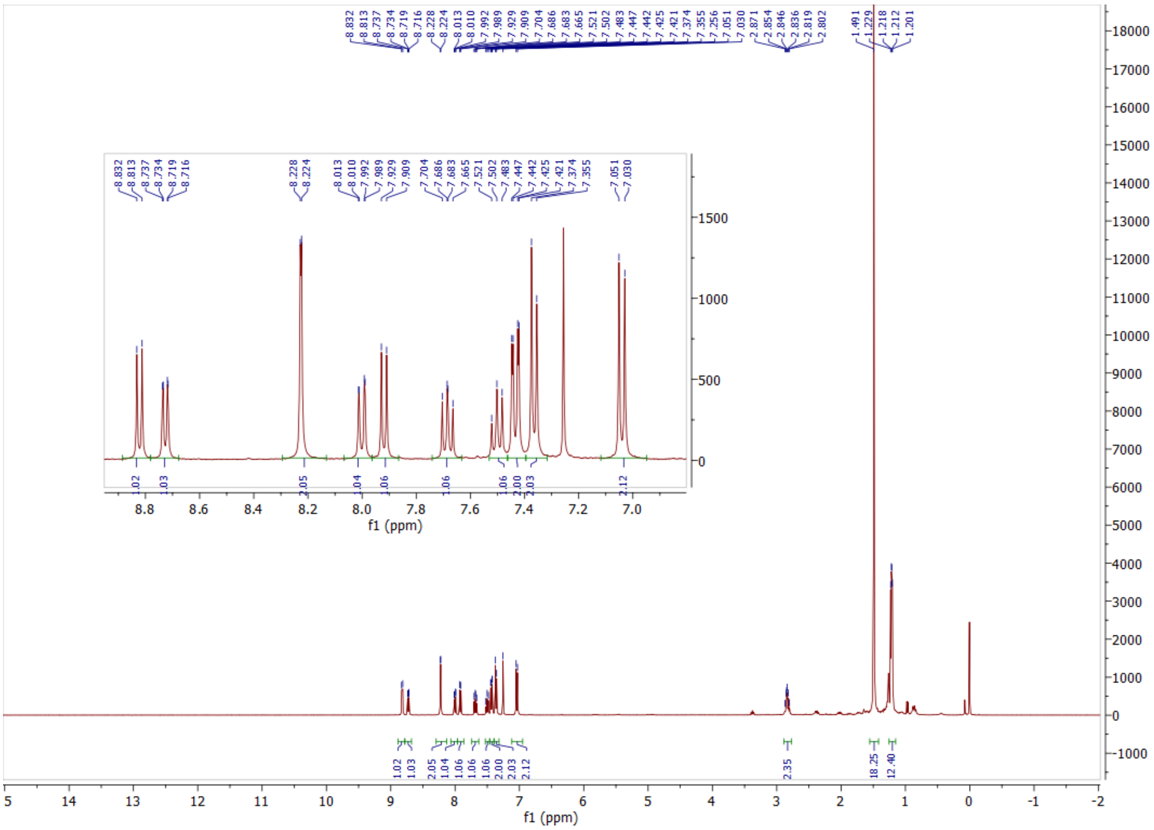

Figure S1. ^{1}H NMR spectrum of **2** (500 MHz, 300K, $CDCl_3$).

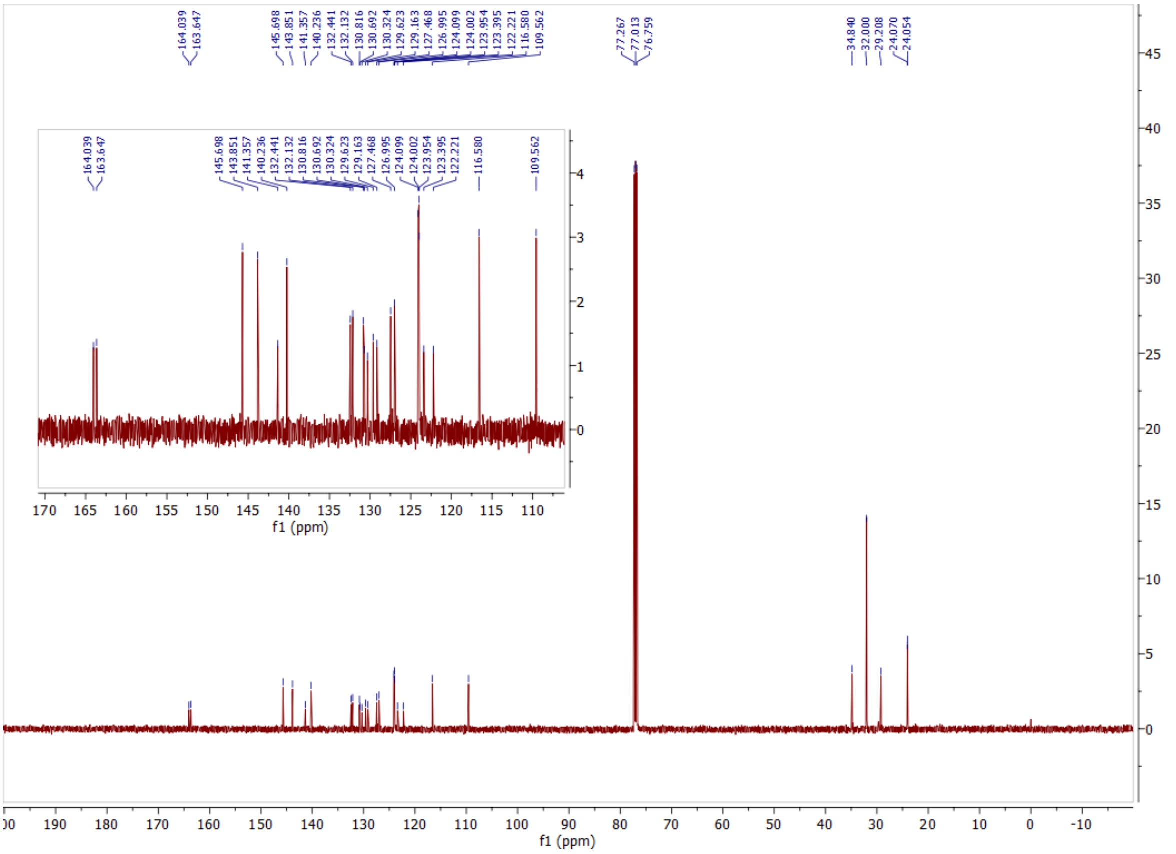

Figure S2. ^{13}C NMR spectrum of **2** (125 MHz, 300K, CDCl$_3$).

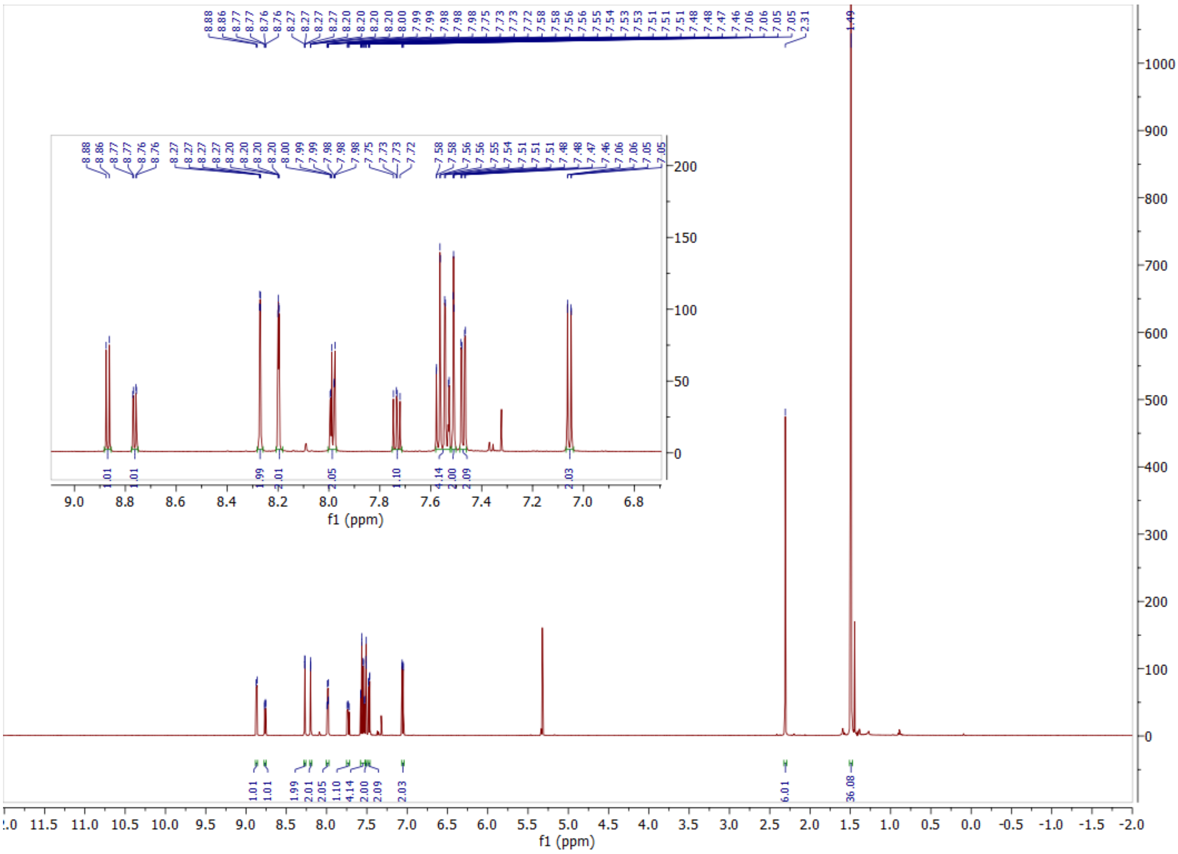

Figure S3. ^{1}H NMR spectrum of **4** (600 MHz, 300K, CD$_2$Cl$_2$).

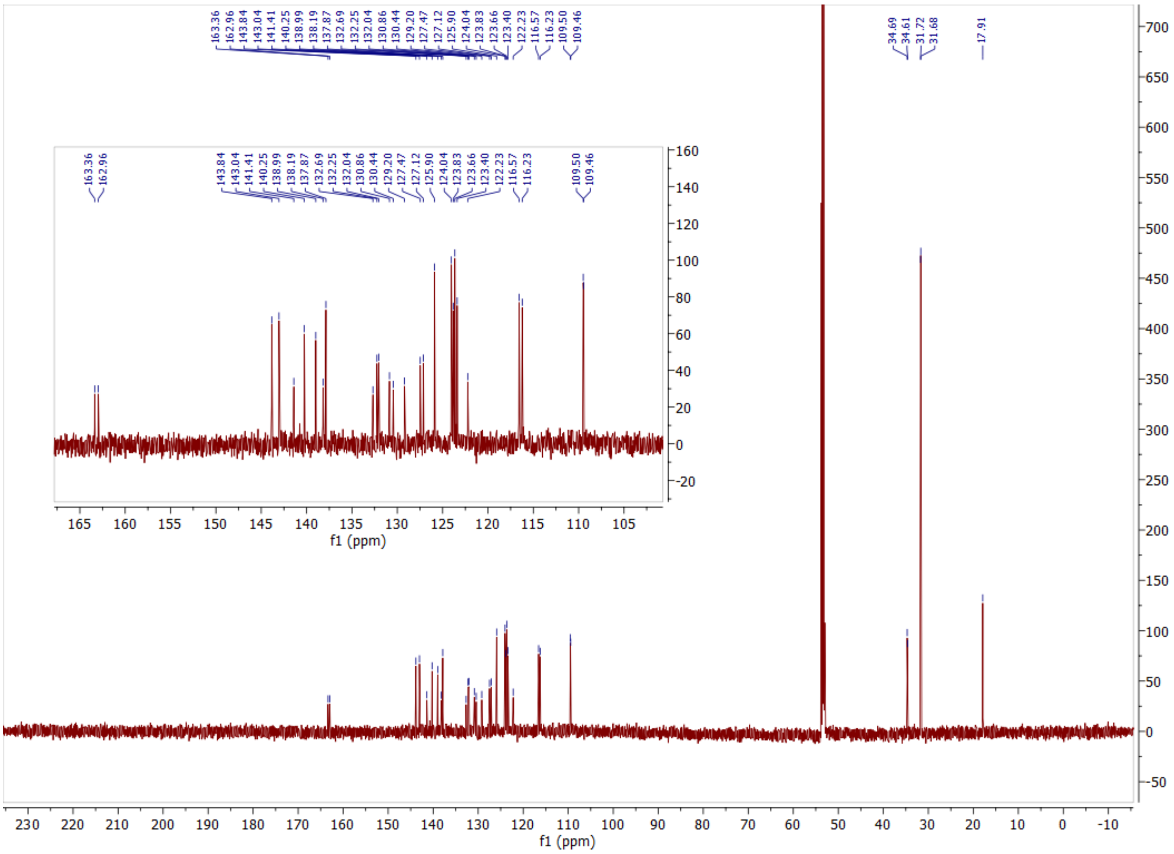

Figure S4. ^{13}C NMR spectrum of **4** (150 MHz, 300K, CD_2Cl_2).

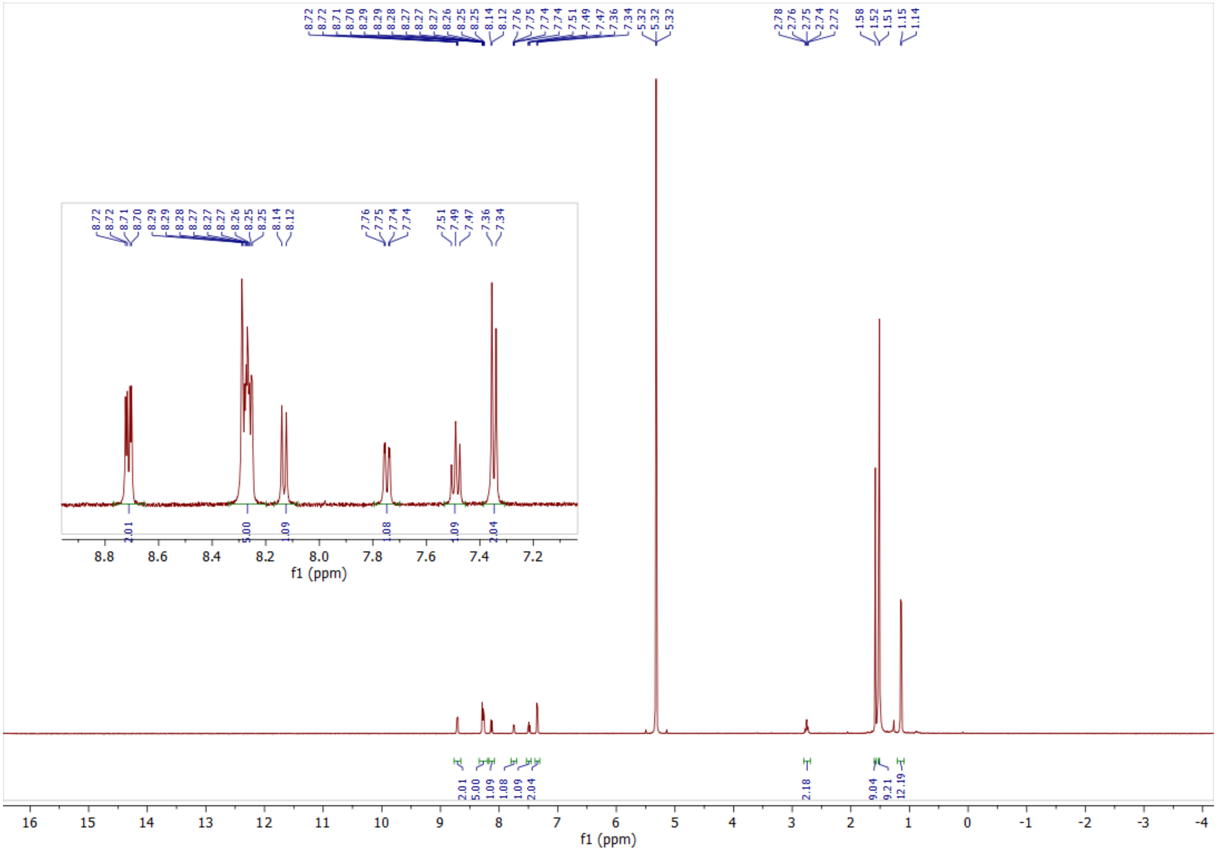

Figure S5. ^{1}H NMR spectrum of **6** (500 MHz, 300K, CD_2Cl_2).

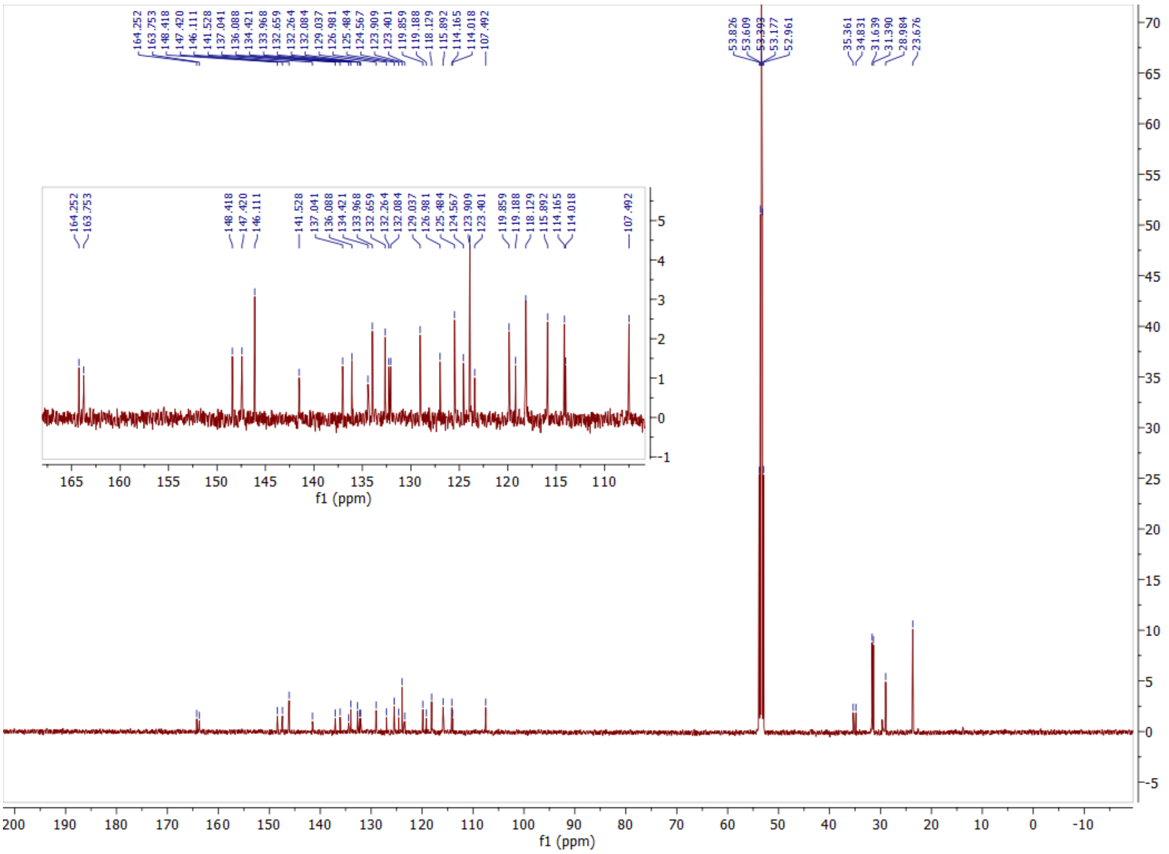

Figure S6. ^{13}C NMR spectrum of **6** (125 MHz, 300K, CD_2Cl_2).

X-Ray analysis

Experimental

The measurements details for compounds **2**, **4**,and **6** are collected in Table S1.

The X-ray measurement of **4** was performed at 130.0(5) K on a Bruker D8 Venture Photon II diffractometer equipped with a TRIUMPH monochromator and a MoKα fine focus sealed tube (λ = 0.71073 Å). A total of 1859 frames were collected with Bruker APEX3 program.[3] The frames were integrated with the Bruker SAINT software package [4] using a narrow-frame algorithm. The integration of the data using an orthorhombic unit cell yielded a total of 67266 reflections to a maximum θ angle of 25.05° (0.84 Å resolution), of which 4597 were independent (average redundancy 14.633, completeness = 99.9%, R_{int} = 5.03%, R_{sig} = 2.59%) and 3797 (82.60%) were greater than $2\sigma(F^2)$. The final cell constants of a = 11.8808(12) Å, b = 10.3821(10) Å, c = 42.031(4) Å, V = 5184.4(9) Å^3, are based upon the refinement of the XYZ-centroids of 575 reflections above 20 $\sigma(I)$ with 5.161° < 2θ<44.34°. Data were corrected for absorption effects using the Multi-Scan method (SADABS)[5]. The ratio of minimum to maximum apparent transmission was 0.816. The calculated minimum and maximum transmission coefficients (based on crystal size) are 0.968 and 0.993.

The structure was solved and refined using SHELXTL Software Package [6,7] using the space group *Pbcn*, with Z = 4 for the formula unit, $C_{63.40}H_{61}N_3O_2$. The final anisotropic full-matrix least-squares refinement on F^2 with 554 variables converged at $R1$ = 9.77%, for the observed data and $wR2$ = 28.77% for all data. The goodness-of-fit was 1.080. The largest peak in the final difference electron density synthesis was 0.386 e$^-$/Å^3 and the largest hole was -0.219 e$^-$/Å^3 with an RMS deviation of 0.053 e$^-$/Å^3. On the basis of the final model, the calculated density was 1.149 g/cm^3 and $F(000)$, 1914 e$^-$. The details concerning the crystal data and structural parameters of **4** are collected in Table S1.

The main molecule, heaving the identity as the only symmetry element, is located on 2-fold axis what causes symmetry-imposed disorder. Because of the additional disorder of the central part of the molecule the moiety is located in four different positions with refined occupancy ratio yielding 0.354(11):0.146(11):0.354(11):0.146(11). Moreover, also the *tert*-butyl fragments in the carbazole unit are disordered over two sites with refined occupancy ratio equal to 0.833(7):0.167(7) and 0.683(8):0.317(8) for C37-C40 and C41-C43 groups respectively. In these moieties C37 and C41 atoms are common for both sites. Furthermore, the structure contains severely disordered unknown solvent species modelled as partial and low occupancy isolated carbon atoms located close to or on the 2-fold axis of symmetry. This results in nonstoichiometric formula of the refined structure. The molecular view of the molecule is presented in Figure S7 a**)**.

All main residue non-hydrogen atoms were refined anisotropically. All hydrogen atoms were placed in calculated positions and refined within the riding model. To preserve reasonable geometry of the disordered molecule number of distance, angle and ADP restraints were used. The temperature factors of hydrogen atoms were not refined and were set to be 1.2 or 1.5 times larger than U_{eq} of the corresponding heavy atom. The atomic scattering factors were taken from the International Tables [8]. Molecular graphics was prepared using program Mercury 4.1 [9]. Thermal ellipsoids parameters are presented at 20% probability level in Figure S7 b).

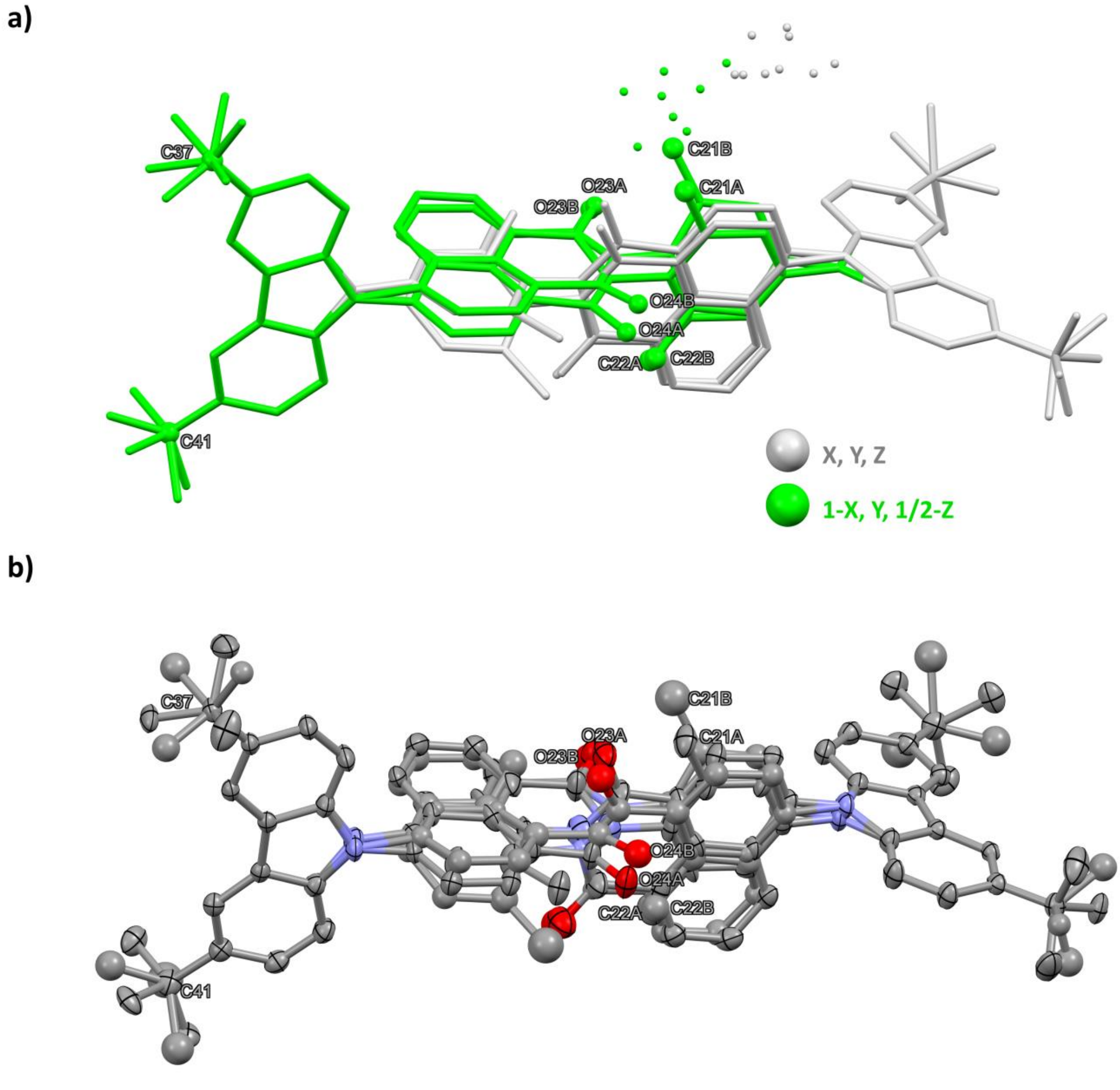

Figure S7. Molecular view of the **4** together with disordered solvent species displayed as separated spheres; **a)** different colors used to show symmetry related parts of the molecule, hydrogen atoms omitted for clarity; **b)** thermal ellipsoid plot at 20% probability level together with numbering scheme of selected atoms in the structure of **4**, hydrogen atoms and disordered solvent moieties omitted for clarity.

Table S1. Crystallographic data of compounds **2, 4** and **6**.

Compound number	**2**	**4**	**6**
CCDC number	2177236	2172685	2122258
Empirical formula	$C_{44}H_{46}N_2O_2$	$C_{63.4}H_{61}N_3O_2$	$C_{45}H_{46}Cl_2N_2O_2$
Formula weight	634.83	896.95	717.74
Temperature/K	293(2)	130.0(5)	100.01(10)
Crystal system	monoclinic	orthorhombic	triclinic
Space group	$P2_1/c$	Pbcn	P-1
a/Å	17.2674(6)	11.8808(12)	8.6461(2)
b/Å	9.7620(3)	10.3821(10)	14.5796(3)
c/Å	22.2538(7)	42.031(4)	15.3848(3)
α/°	90.00	90	99.024(2)
β/°	108.270(3)	90	95.585(2)
γ/°	90.00	90	104.779(2)
Volume/Å^3	3562.1(2)	5184.4(9)	1832.73(7)
Z	4	4	2
ρ_{calc}g/cm^3	1.184	1.149	1.301
μ/mm^{-1}	0.555	0.069	1.911
F(000)	1360.0	1914.0	760.0
Crystal size/mm^3	0.1 x 0.03 x 0.01	0.476 × 0.356 × 0.103	0.4 × 0.2 × 0.06
Radiation	CuKα (λ = 1.54184)	MoKα (λ = 0.71073)	CuKα (λ = 1.54184)
2Θ range for data collection/°	5.38 to 141.34	5.18 to 50.1	6.38 to 141.18
Index ranges	-19 ≤ h ≤ 21, -11 ≤ k ≤ 9, -25 ≤ l ≤ 27	-14 ≤ h ≤ 14, -12 ≤ k ≤ 12, -49 ≤ l ≤ 50	-10 ≤ h ≤ 10, -17 ≤ k ≤ 17, -18 ≤ l ≤ 18
Reflections collected	22025	67266	32944
Independent reflections	6805 [R_{int} = 0.0374, R_{sigma} = 0.0359]	4597 [R_{int} = 0.0503, R_{sigma} = 0.0259]	6987 [R_{int} = 0.0296, R_{sigma} = 0.0164]
Data/restraints/parameters	6805/0/464	4597/266/554	6987/18/501
Goodness-of-fit on F^2	1.034	1.080	1.060
Final R indexes [I>=2σ (I)]	R_1 = 0.1048, wR_2 = 0.2902	R_1 = 0.0977, wR_2 = 0.2757	R_1 = 0.0397, wR_2 = 0.1099
Final R indexes [all data]	R_1 = 0.1223, wR_2 = 0.3047	R_1 = 0.1093, wR_2 = 0.2877	R_1 = 0.0404, wR_2 = 0.1105
Largest diff. peak/hole / e Å^{-3}	2.47/-0.76	0.39/-0.22	0.38/-0.42

Preliminary DFT and TDDFT calculations

Calculation Setup

In this section, we report the results of the preliminary time-dependent density functional theory (TDDFT) calculations, which we used to obtain a rough picture of the photophysics of compounds **2**, **4**, and **6**. Unlike the subsequent SOS-ADC(2) calculations, the TDDFT calculations were performed for the complete molecules of these compounds; we did not resort to using truncated model compounds **7** and **8**.

The ground electronic states of the compounds under study were described with the use of density functional theory (DFT), while their excited electronic states were treated with linear-response TDDFT. We elected to use the long-range corrected functional ωB97XD, [10] as this functional has previously been shown to provide reasonably accurate excitation energies for intramolecular charge transfer (ICT) states of organic donor-acceptor systems.[11–13] At the same time, however, TDDFT is unreliable for the calculation of singlet-triplet gaps,[14–17] which is our main motivation for later switching to the SOS-ADC(2) method.

The def2-SVP basis set[18] was used. The Tamm-Dancoff approximation[19] (TDA) was employed a cost-reducing measure. All calculations were performed in vacuo, which is to say, for isolated molecules. The DFT and TDDFT calculations were performed with the computational chemistry software package Gaussian 16, Revision A.03.[20]

The vertical emission energies of the compounds under study were evaluated at the appropriate excited-state equilibrium geometries – that is to say, the minimum on the potential energy surface (PES) of the S_1 state for fluorescence emission, and the minimum on the PES of the T_1 state for phosphorescence emission. The calculated vertical emission energies and the magnitudes of the electric dipole moments of the excited-state structures are given in Table S1. For ease of reference, Table S1 also lists the magnitudes of these compounds' ground-state electric dipole moments. Accompanying this data, Figure S1 shows the EDDMs for the S_1 and T_1 states at the respective excited-state equilibrium geometries (S_1-min and T_1-min).

Table S2: Optical and electronic properties of the ground- and excited-state structures of compounds **2**, **4**, and **6** as calculated at the TD-ωB97XD/def2-SVP level of theory: vertical emission energies (ΔE) and electric dipole moments (μ). The diabatic character of the given excited state at the excited-state equilibrium geometry is given in brackets. Also listed are oscillator strengths for vertical fluorescence emission (f).

Compound	Structure	ΔE, eV	f	μ, D
2	S_0-min			3.8
	S_1-min (D1 → A ICT)	2.995	$< 1 \times 10^{-4}$	21.9
	T_1-min (A ππ*)	1.977		6.1
4	S_0-min			5.6
	S_1-min (D1 → A ICT)	2.981	1×10^{-4}	24.7
	T_1-min (A ππ*)	1.978		8.1
6	S_0-min			7.9
	S_1-min (D1 + A ππ*)	3.041	0.944	9.5
	T_1-min (D1 + A ππ*)	1.831		7.7

For compounds **2** and **4**, the S_1-min geometries are characterized by ICT from the D1 moiety onto the A moiety. Both these compounds exhibit very low oscillator strengths for fluorescence emission. In the case of the rigidized compound **6**, the S_1 state at the minimum-energy geometry is delocalized over both the D1 and the A moieties and lacks an ICT character. Its oscillator strength for fluorescence emission is appreciably large, at 0.944. The above results are consistent with the fact that compounds **2** and **4** show strong solvatofluorochromism, whereas the fluorescence emission from **6** is rather insensitive to the choice of the solvent.

(a) **2**

(i) S_1 state at S_1-min (ii) T_1 state at T_1-min

(b) **4**

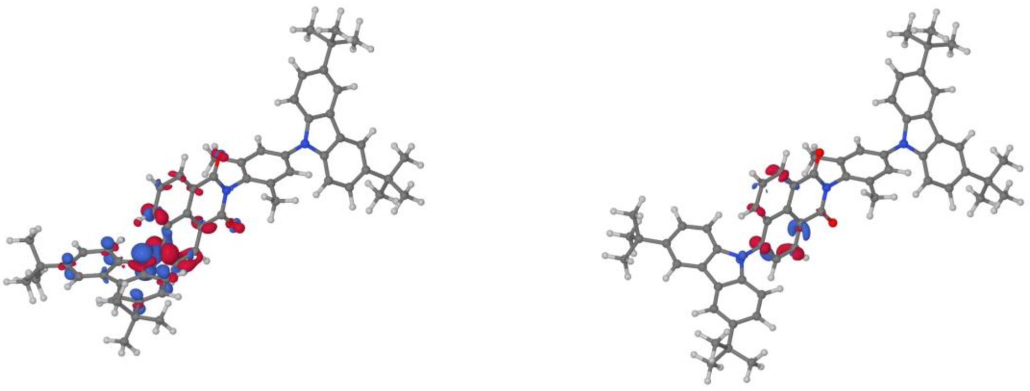

(i) S_1 state at S_1-min (ii) T_1 state at T_1-min

(c) **6**

(i) S_1 state at S_1-min (ii) T_1 state at T_1-min

Figure S8: EDDMs for the S_1 and T_1 states of compounds **2**, **4**, and **6** at their respective excited-state equilibrium geometries, calculated at the TD-ωB97XD/def2-SVP level of theory. The EDDMs are plotted in the form of isosurfaces with isovalues of ±0.005 e/a_0^3 . The red and blue isosurfaces delimit regions in which the electron density is increased and decreased, respectively, relative to the S_0 state.

As regards phosphorescence emission, in compounds **2** and **4** phosphorescence is predicted to take place from T_1 states localized on the A moiety. The inspection of the EDDMs of these states shows that they are essentially counterparts of the T_1 ($^3B_{2u}$) state of unsubstituted naphthalene, which is dominated by a HOMO→LUMO excitation.[21] Due to the close similarity of the electronic structures of the T_1 states of **2** and **4**, the calculated vertical phosphorescence emission energies calculated for these two compounds coincide with one another almost exactly. In compound **6**, on the other hand, the T_1 state is delocalized over the near-coplanar D1 and A moieties, and the vertical phosphorescence emission energy is somewhat lower than for **2** and **4**.

In all three compounds, the phenylene linker (L) and, in the case of compound **4**, the second donor moiety (D2), are not directly involved in the low-lying excited states. It follows that the photophysical properties of these compounds can be examined with the use of truncated model compounds in which the L moiety (along with the D2 moiety in the case of compound **4**) is replaced with a hydrogen atom. This paves the way for the application of the SOS-ADC(2) method, which is computationally more demanding, but it is expected to be more accurate than TDDFT for the relative energies of various excited-state structures, and for singlet-triplet gaps.

Technical details of SOS-ADC(2) and ACID computations.

The SOS-ADC(2) calculations were performed with the program Turbomole, version 6.3.1,[22] taking advantage of the frozen core and resolution of the identity [23-26] approximations. A restricted Hartree-Fock (RHF) reference determinant was always used. The cc-pVDZ basis set [27] was employed in combination with the default auxiliary basis set.[28] The singlet ground state was described with the spin-opposite-scaled Møller-Plesset perturbation method of second order (SOS-MP2).[29] The SOS-MP2 method was also used to optimize the ground-state equilibrium geometries of the model compounds.

The electronic structures of the relevant excited electronic states were characterized by plotting electron density difference maps (EDDMs). An EDDM is defined simply as the difference of the electron density of the excited state and that of the ground state at the same nuclear geometry. Thus, the EDDM shows the redistribution of electron density due to a vertical transition.

To examine how the additional linkage between the D and A moieties in compound **6** affects its π-bonding system, we characterized the singlet ground state of model compound **8** with the use of the anisotropy of the current (induced) density (ACID) method.[30,31] In this approach, electron delocalization is associated with appreciably large values of the ACID scalar field. In particular, conjugated systems are considered aromatic if they exhibit strong diatropic ring currents in the π-bonding region.[30,31]

For the purposes of the ACID analysis, the ground-state equilibrium geometry of compound **8** was reoptimized at the density functional theory (DFT) level with the imposition of *Cs* symmetry. Constraining the molecule to *Cs* symmetry is not strictly necessary, but it does simplify the subsequent analysis by ensuring that the molecule adopts a planar geometry. The DFT calculations were performed within the computational chemistry software package Gaussian 16, Revision A.03.[32] The B3LYP exchange-correlation functional [33] was employed in combination with the def2-SVP basis set.[34] The subsequent ACID analysis was carried out using the program of Geuenich and coworkers[31], which contains an interface to Gaussian 16. As per usual practice, the total ACID was separated into contributions from the σ and the π orbitals, from which we examine total ACID as well as the contribution from the π orbitals.

(a) compound **7**

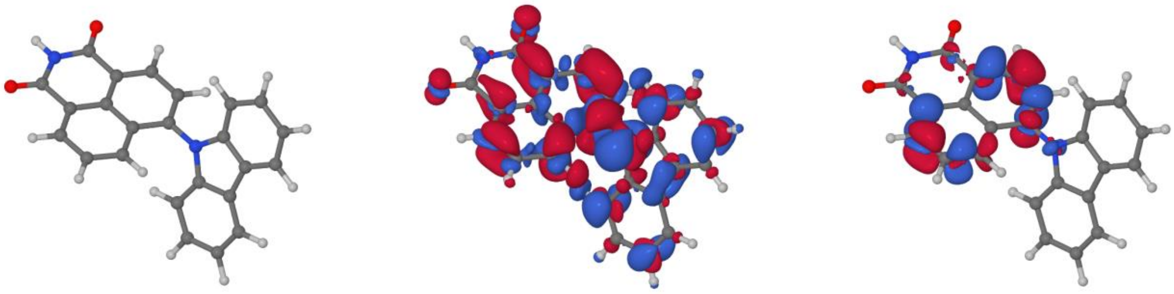

(i) ground-state geometry (ii) EDDM for S_1 (D → A ICT) state (iii) EDDM for T_1 (A ππ*) state

(b) compound **8**

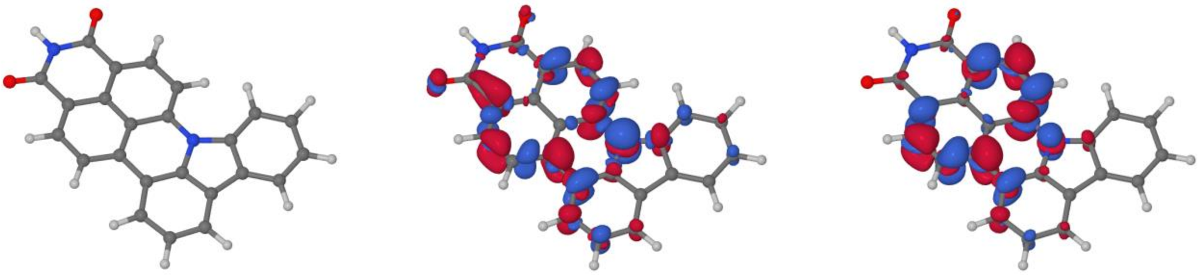

(i) ground-state geometry (ii) EDDM for S_1 (D + A ππ*) state (iii) EDDM for T_1 (D + A ππ*) state

Figure S9: Ground-state equilibrium geometries of model compounds **7**(a) and **8**(b) as optimized at the SOS-MP2/cc-pVDZ level of theory. For both compounds, the lowest singlet and triplet excited state is characterized by plotting its EDDM. The EDDMs are plotted in the form of isosurfaces with isovalues of ±0.002 e/a_0^3 . The red and blue isosurfaces describe regions in which the electron density is increased and decreased, respectively, relative to the S_0 state.

Photophysics

Experimental

UV-vis spectra were recorded on a Shimadzu UV-2550 spectrophotometer. Steady-state emission spectra were recorded on a Jobin Yvon Horiba Fluoromax 3, with solvent studies performed in clean 1 cm path-length photoluminescence cuvettes (Arieka Cells) and temperature dependent film photoluminescence films studies performed on within a liquid N_2 cooled cryostat (Janis Research). Photoluminescence spectra were calibrated for detector efficiency using company supplied, instrument specific calibration files. The emitter materials were also degassed in toluene solvent using a custom made 1 cm path-length degassed cell stoppered with a Young tap and degassed using 5 freeze/thaw/pump cycles. The photoluminescence quantum yield (PLQY) of emitters in toluene solvent was determined using the reference method against 9,10-diphenylanthracene (DPA). Solid-state samples were prepared as 1% w/w ratio emitters in Zeonex® polymer host on clean/dry sapphire disc substrates. Phosphorescence, prompt fluorescence (PF), and delayed fluorescence (DF) spectra and decays were recorded using nanosecond gated luminescence and lifetime measurements (from 400 ps to 1 s) using either third harmonics of a high energy pulsed DPSS laser emitting at 355 nm (Q-Spark A50-TH-RE). Emission was focused onto a spectrograph and detected on a sensitive gated iCCD camera (Stanford Computer Optics) having a sub-nanosecond resolution. PF/DF time-resolved measurements were performed by exponentially increasing gate and integration times. Temperature-dependent experiments were conducted using an helium cryostat (Janis Research) under a vacuum.

Time-resolved measurements were performed by exponentially increasing the gate and delay times of iCCD Stanford Computer Optics 4Picos camera from laser excitation. The delay and integration times are set at a time longer than the previous sum of delay and integration time to avoid overlap. As the next step, the curve is corrected by integrating the measured spectra to obtain proper luminescence decay profile. Every point represents the collected emission spectra of respective emitting specie.

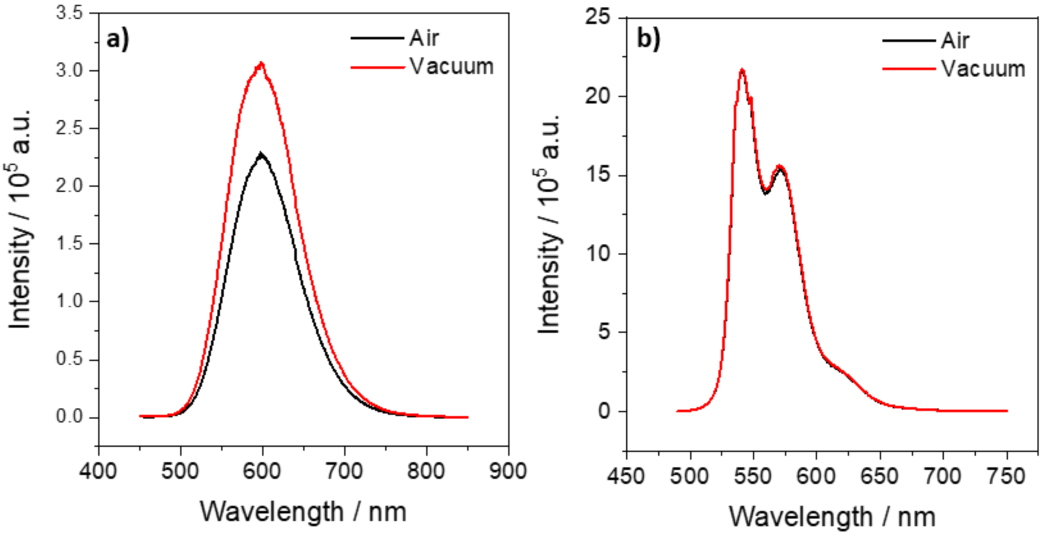

Figure S10. Emission spectra of compound a) **2** and b) **6** under air (black) and vacuum (red) conditions. Solid samples contain 1 wt% of compound **2**/**6** in Zeonex® matrix (λex = 355 nm).

Devices

Experimental

NPB (*N*,*N*′-di(1-naphthyl)-*N*,*N*′-diphenyl-(1,1′-biphenyl)-4,4′-diamine) was used as a Hole Injection Layer (HIL) and Hole Transport Layer (HTL), TAPC (4,4′-Cyclohexylidenebis[*N*,*N*-bis(4-methylphenyl)benzenamine]) were used as a Electron Blocking Layer (EBL). TPBi 2,2’,2”-(1,3,5-Benzinetriyl)-tris(1-phenyl-1-H-benzimidazole) was introduced as an Electron Transport Layer (ETL). Lithium fluoride (LiF) and aluminium were used as the cathode. Organic semiconductors and aluminium were deposited at a rate of 1 Ås-1, and the LiF layer was deposited at 0.1 Ås-1. mCP1,3-Bis(carbazol-9-yl)benzene was used as hosts for all emitters. All materials were purchased from Sigma Aldrich or Lumtec and were purified by temperature-gradient sublimation in a vacuum. OLEDs have been fabricated on pre-cleaned, patterned indium-tin-oxide (ITO) coated glass substrates with a sheet resistance of 20 Ω/sq and ITO thickness of 100 nm. All small molecules and cathode layers were thermally evaporated in a Kurt J. Lesker SuperSpectros 200 evaporation system under pressure of 10^{-7} mbar without breaking the vacuum. The sizes of pixels were 4 mm^2, 8 mm^2 and 16 mm^2. Each emitting layer has been formed by co-deposition of dopant and host at the specific rate to obtain 10% content of the emitter. The characteristics of the devices were recorded using a 6-inch integrating sphere (Labsphere) inside the glovebox connected to a Source Meter Unit and Ocean Optics USB4000 spectrometer.

Electrochemistry

Experimental

Electrochemical measurements were performed in 0.1 M Bu_4NBF_4 (99%, Sigma Aldrich, dried) in dichloromethane (CHROMASOLV®, 99.9% Sigma Aldrich). Solutions were purged with argon prior to measurement. Electrodes: working (Pt disc 1 mm of diameter), counter (Pt wire), reference (Ag/AgCl calibrated against ferrocene).

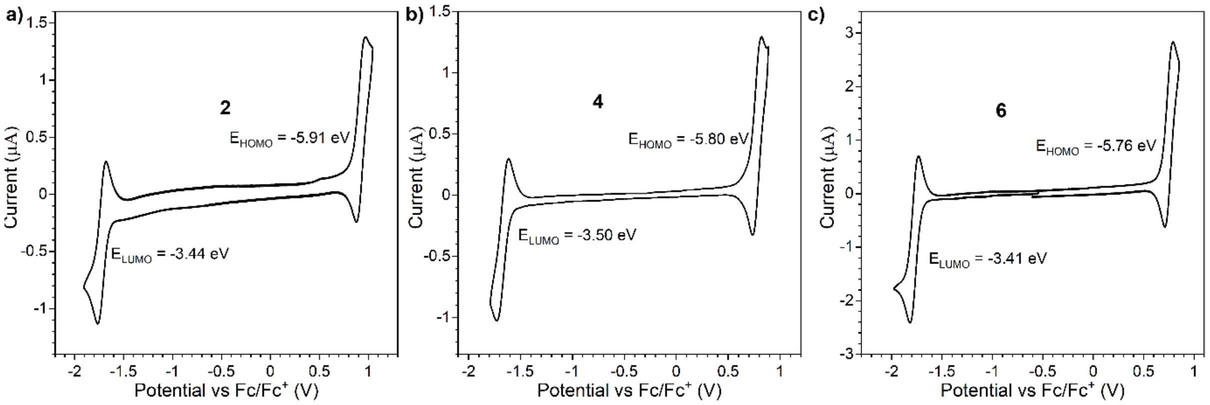

Figure S11. CV of 1 mM of emitters in 0.1 M Bu_4NBF_4 in DCM electrolyte at the scan rate of 50 mV/s.

References

[1] Y. Hashikawa, M. Murata, A. Wakamiya, Y. Murata, *J. Am. Chem. Soc.*, **2017**, *139*, 16350–16358.
[2] D. Uersfeld, S. Stappert, C. Li, K. Müllen, *Advanced Synthesis & Catalysis*, **2017**, *359*, 4184–4189.
[3] APEX3 V2019, Bruker Nano, Inc., **2019**.
[4] SAINT V8.40A, Bruker Nano, Inc., **2019**.
[5] SADABS V2016/2, Bruker Nano, Inc., 2019.
[6] G. M. Sheldrick, *Acta Cryst.*, **2015**, *A71*, 3-8.
[7] G. M. Sheldrick, *Acta Cryst.*, **2015**, *C71*, 3–8.
[8] *International Tables for Crystallography*, Ed. A. J. C. Wilson, Kluwer:Dordrecht, **1992**, Vol.C.
[9] C. F. Macrae, I. J. Bruno, J. A. Chisholm, P. R. Edgington, P. McCabe, E. Pidcock, L. Rodriguez-Monge, R. Taylor, J. van de Streek and P. A. Wood, "Mercury CSD 2.0 - New Features for the Visualization and Investigation of Crystal Structures", *J. Appl. Cryst.*, **2008**, 41, 466-470.
[10] J.-D. Chai, M. Head-Gordon, *Phys. Chem. Chem. Phys.* **2008**, *10*, 6615–6620.
[11] P. Xu, C.-R. Zhang, W. Wang, J.-J. Gong, Z.-J. Liu, H.-S. Chen, *Int. J. Mol. Sci.* **2018**, *19*, 1134
[12] Y. Jiang, Z. Hu, B. Zhou, C. Zhong, Z. Sun, H. Sun, *J. Phys. Chem. C* **2019**, *123*, 5616–5625.
[13] Y. Shao, Y. Mei, D. Sundholm, V. R. I. Kaila, *J. Chem. Theory Comput.* **2020**, *16*, 587–600.
[14] P. de Silva, *J. Phys. Chem. Lett.* **2019**, *10*, 5674–5679.
[15] J. Ehrmaier, E. J. Rabe, S. R. Pristash, K. L. Corp, C. W. Schlenker, A. L. Sobolewski, W. Domcke, *J. Phys. Chem. A* **2019**, *123*, 8099–8108.
[16] G. Ricci, E. San-Fabián, Y. Olivier, J. C. Sancho-García, *ChemPhysChem* **2021**, *22*, 553–660.
[17] S. Ghosh, K. Bhattacharyya, *J. Phys. Chem. A* **2022**, *126*, 1378–1385.
[18] F. Weigend, R. Ahlrichs, *Phys. Chem. Chem. Phys.* **2005**, *7*, 3297–3305.
[19] S. Hirata, M. Head-Gordon, *Chem. Phys. Lett.* **1999**, *314*, 219–299.

[20] Gaussian 16, Revision A.03, M. J. Frisch, G. W. Trucks, H. B. Schlegel, G. E. Scuseria, M. A. Robb, J. R. Cheeseman, G. Scalmani, V. Barone, G. A. Petersson, H. Nakatsuji, X. Li, M. Caricato, A. V. Marenich, J. Bloino, B. G. Janesko, R. Gomperts, B. Mennucci, H. P. Hratchian, J. V. Ortiz, A. F. Izmaylov, J. L. Sonnenberg, D. Williams-Young, F. Ding, F. Lipparini, F. Egidi, J. Goings, B. Peng, A. Petrone, T. Henderson, D. Ranasinghe, V. G. Zakrzewski, J. Gao, N. Rega, G. Zheng, W. Liang, M. Hada, M. Ehara, K. Toyota, R. Fukuda, J. Hasegawa, M. Ishida, T. Nakajima, Y. Honda, O. Kitao, H. Nakai, T. Vreven, K. Throssell, J. A. Montgomery, Jr., J. E. Peralta, F. Ogliaro, M. J. Bearpark, J. J. Heyd, E. N. Brothers, K. N. Kudin, V. N. Staroverov, T. A. Keith, R. Kobayashi, J. Normand, K. Raghavachari, A. P. Rendell, J. C. Burant, S. S. Iyengar, J. Tomasi, M. Cossi, J. M. Millam, M. Klene, C. Adamo, R. Cammi, J. W. Ochterski, R. L. Martin, K. Morokuma, O. Farkas, J. B. Foresman, and D. J. Fox, Gaussian, Inc., Wallingford CT, 2016.
[21] T. Hashimoto, H. Nakano, K. Hirao, *J. Chem. Phys.* **1996**, 104, 6244–6258.
[22] TURBOMOLE V6.3.1 2011, a development of University of Karlsruhe and Forschungszentrum Karlsruhe GmbH (1989-2007), and TURBOMOLE GmbH (since 2007). Available from: http://www.turbomole.com
[23] A. Köhn and C. Hättig, *The Journal of Chemical Physics*, **2003**, *119*, 5021–5036.
[24] F. Haase and R. Ahlrichs, *Journal of Computational Chemistry*, **1993**, *14*, 907–912.
[25] F. Weigend and M. Häser, *Theoretical Chemistry Accounts*, , DOI:10.1007/s002140050269.
[26] C. Hättig and F. Weigend, *The Journal of Chemical Physics*, **2000**, *113*, 5154.
[27] T. H. Dunning, *The Journal of Chemical Physics*, **1989**, *90*, 1007–1023.
[28] F. Weigend, A. Köhn and C. Hättig, *Journal of Chemical Physics*, DOI:10.1063/1.1445115.
[29] Y. Jung, R. C. Lochan, A. D. Dutoi and M. Head-Gordon, *The Journal of Chemical Physics*, **2004**, *121*, 9793–9802.
[30] R. Herges and D. Geuenich, *Journal of Physical Chemistry A*, DOI:10.1021/jp0034426.
[31] D. Geuenich, K. Hess, F. Köhler and R. Herges, *Chemical Reviews*, **2005**, *105*, 3758–3772.
[32] T. H. Dunning, *The Journal of Chemical Physics*, , DOI:10.1063/1.456153.
[33] A. D. Becke, *The Journal of Chemical Physics*, **1993**, *98*, 5648–5652.
[34] F. Weigend and R. Ahlrichs, *Physical Chemistry Chemical Physics*, **2005**, *7*, 3297.